X-RAY TOPOGRAPHIC STUDY ON DISLOCATIONS INDUCED BY LASER IRRADIATION

AKASHI, Yoshito
Research Institute for Applied Mechanics, Kyushu University

https://doi.org/10.5109/7173524

出版情報：Reports of Research Institute for Applied Mechanics. 23 (74), pp.99-107, 1975. 九州大学応用力学研究所
バージョン：
権利関係：

Reports of Research Institute for Applied Mechanics
Vol. XXIII, No. 74, 1975

X-RAY TOPOGRAPHIC STUDY ON DISLOCATIONS INDUCED BY LASER IRRADIATION

By Yoshito AKASHI*

Dislocations induced by laser irradiation is studied by x-ray diffraction topography on lithium fluoride single crystal. These dislocations are composed of four types of glissile dislocations in half-loops, (101) [$10\bar{1}$], ($\bar{1}01$) [$\bar{1}0\bar{1}$], (011) [$01\bar{1}$] and ($0\bar{1}1$) [$0\bar{1}\bar{1}$].

1. Introduction

We are able to introduce dislocations into crystals by irradiating {100} surface of lithium fluoride with high intensity laser pulse[1]. In the specimen irradiated by the laser pulse with power density of $\sim$4 MW/4.5 mmϕ, the density of induced dislocations are so small that individual dislocations are observable on limited projection topograph. To determine the geometry of induced dislocations a series of topographs utilizing various diffraction planes was taken, and the invisibility criterion for dislocation image and the geometry of possible dislocation and x-ray projection were taken into account.

2. Experimental

The laser used was a hand-made CO_2 laser system in Research Institute for Applied Mechanics[2]. The parameters of laser pulse were $\sim$2.5 J in 80 nsec. The lens of 500 mm focal length was used to intensify the power density of irradiation. The specimen used, $5\times7\times2\,mm^3$ in size with $\sim10^4$ dislocations/cm^2, were cleaved from lithium fluoride single crystal block of x-ray analyzing grade purchased from Harshaw Chemical Company. The power density of irradiation for the studied specimen was $\sim$4MW/4.5 mmϕ. Utilizing the limited projection topography[3),4)], (200), ($\bar{2}00$), ($0\bar{2}0$), (020), (220), (202), ($\bar{2}02$), (022) and ($0\bar{2}2$) topographs were taken. As the MoKα_1 radiation was used, $\mu t<1$ where μ is the linear absorption coefficient of specimen and t is its thickness. Ilford L4 nuclear plate was used.

---

* Research Associate, Research Institute for Applied Mechanics, Kyushu University.

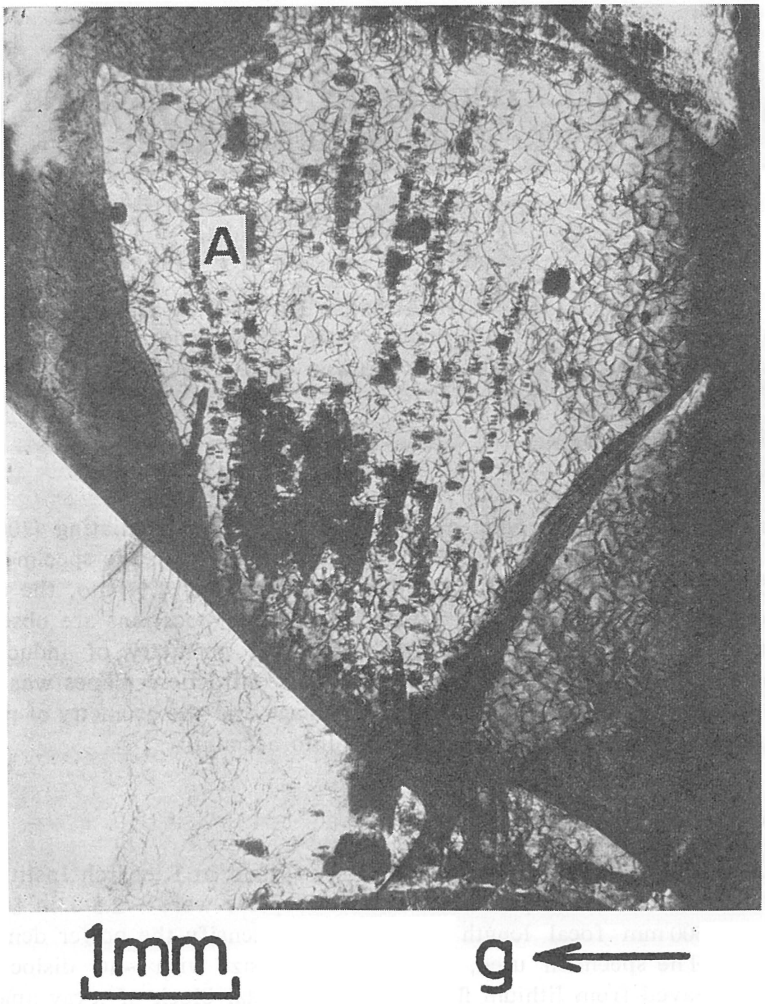

Photo 1 ($\bar{2}00$) topograph of the laser irradiated specimen. Loops and half-loops of dislocation are induced over the irradiated surface.

3. Results

A ($\bar{2}00$) topograph of specimen is shown in Photo 1. Dislocations in loops and half-loops are induced over the irradiated surface. In ($\bar{2}00$) topograph taken before laser irradiation no such loops were observed. Topographs taken with various diffraction vectors are listed in Photo 2, where the region below the letter A in Photo 1 is shown. Distinctive features of induced dislocations on topographs with various diffraction vectors are as follows.

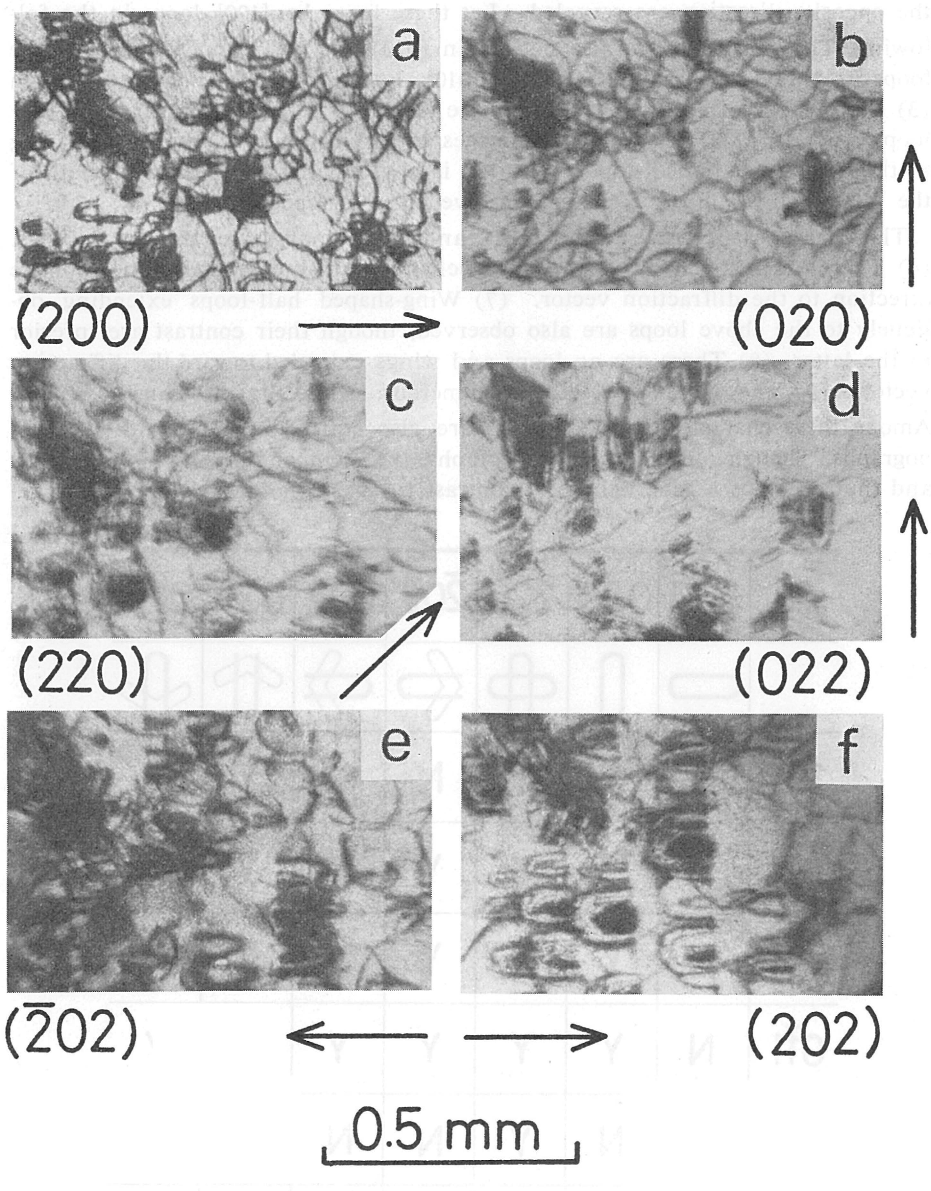

Photo 2 A series of topographs with various diffraction vectors. Each arrow shows diffraction vector used.

In (200) and ($\bar{2}$00) topographs (1) there are no essential differences in dislocation images and (2) loops and half-loops along diffraction vector and in the opposite direction are revealed. Let these loops be [100] loops in the following. These features are also noticed in (020) and (0$\bar{2}$0) topographs. As the loops in these topographs are along [010], let them be [010] loops. Though (3) the number of [010] loops are quite small comparing with that of [100] loops. (4) In (220) topograph the images of dislocation were faint comparing to the above mentioned topographs. It is obvious, however, that (5) both of the [100] and the [010] loops are observed in this topograph.

The characteristics revealed in (202) and ($\bar{2}$02) topographs are as follows. (6) There are many half-loops, with excellent contrast, extended in the opposite direction to the diffraction vector. (7) Wing-shaped half-loops extending obliquely to the above loops are also observed, though their contrast are inferior to the latter. (8) There are no loops and wings extended toward the diffraction vector. (9) The number of loops is numerous, while that of wings is a few. Among these characteristics (6) to (8) are also noticed in (022) and (0$\bar{2}$2) topographs. Though (10) in these topographs the number of wings is numerous and that of loops a few, being in contrast to (9). Photo 2 (d) shows the re-

g	200	020	220	$\bar{2}$02	202	022	0$\bar{2}$2
	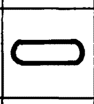	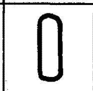	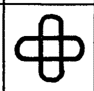	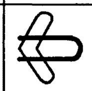	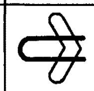	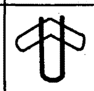	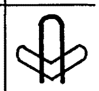
101	Y	N	Y	N	Y	Y	Y
$\bar{1}$01	Y	N	Y	Y	N	Y	Y
011	N	Y	Y	Y	Y	Y	N
0$\bar{1}$1	N	Y	Y	Y	Y	N	Y
100	Y	N	Y	N	N	Y	Y
010	N	Y	Y	Y	Y	N	N

Table 1 Distinctive features of each topographs are summarized with the list of visibility of dislocations with various Burgers vectors for the used diffraction vector.

gion where most half-loops are contained. The direction along which the half-loops in (202) and (022) topographs are extended is correspond to the direction of [100] loops and [010] loops respectively. (11) Comparing the length of half-loops in (202) and (200) topographs, one can notice that the loops in (202) is longer than ones in (200) and their ratio is 1.8 taking into account the geometry of projection in the direction of loop length. The same ratio is obtained in (020) and (022) topographs. Some of the distinctive features mentioned above are given in the second line in Table 1.

	200	020	220	$\bar{2}02$	202	022	$0\bar{2}2$	b	n
⊃	Ex	No	G	Ex	No	G	G	$\bar{1}01$	101
⊂	Ex	No	G	No	Ex	G	G	101	$\bar{1}01$
∩	No	Ex	G	G	G	No	Ex	$0\bar{1}1$	011
∪	No	Ex	G	G	G	Ex	No	011	$0\bar{1}1$

Table 2 Visibility of four half-loops of dislocation in a series of topographs is tabulated. Determined Burgers vector and crystallographic plane of each half-loop are sited in the last two columns.

4. Discussion

The compressive stress wave is generated in the crystal irradiated by laser pulse[5]. There are two possible dislocations; (a) glide dislocations with Burgers vector, $\boldsymbol{b}=\langle 110\rangle$ generated by the resolved shear stress and (b) punched-in dislocations with $\boldsymbol{b}=\langle 100\rangle$ owing to the local stress concentration. With the help of invisibility criterion observable dislocations (Y) and invisible dislocations (N) are examined for the used diffraction vectors and the result is tabulated in Table 1. The comparison of the experimental results with the examined results excludes Burgers vectors of [110], [$\bar{1}10$] and [001] and they are not included in the table.

As in (202) topograph only the loops extended to the right are visible and in ($\bar{2}02$) only the left are visible, the [100] loop may decomposed into two half-loops extended to the right and to the left respectively. Comparing the characteristics (9) and (10) with the (3) which shows the numerical correlation between the [100] loops and the [010] loops, one can notice that when half-loops corresponding to [100] loops are observed a few wings numerically corresponding to [010] loops are visible, and that when half-loops corresponding to [010] loops are observed a lot of wings numericaly corresponding to [100] loops are visible. Wings shown in (202) and $(\bar{2}02)$ topographs are then reasonably decomposed into two half-loops of [010] and $[0\bar{1}0]$.

Then we have four half-loops extended toward [100], $[\bar{1}00]$, [010] and $[0\bar{1}0]$ respectively. In a series of topographs these four loops are evaluated and classified into three groups; loops with excellent contrast (Ex), loops with good contrast (G) and loops invisible (No). The result is summarized in Table 2. Comparing the Tables 1 and 2, one can determine the Burgers vector of each half-loop and the result is sited in the ***b***'s column in Table 2.

The crystallographic plane on which half-loops are formed will be determined in the following. The possible planes for the dislocations (a) and (b) are {110} and {100}. The wing in (202) topograph is extended at an angle of $\sim$ 60° to $[\bar{1}00]$. If the [010] half-loop is extended on {100} plane this angle must be $\sim$90° while if it is on {110} plane the angle of $\sim$60° is reasonable. The characteristic (11) shows that the ratio of half-loop length on (202) and (200) topographs is 1.8. If the half-loops were extended on (101) plane this ratio must be 0.3 considering the geometry of projection to take topography. If they are on $(\bar{1}01)$, (100) or (001) plane, this ratio should be 1.7, 2.9 or 0.9 respec-

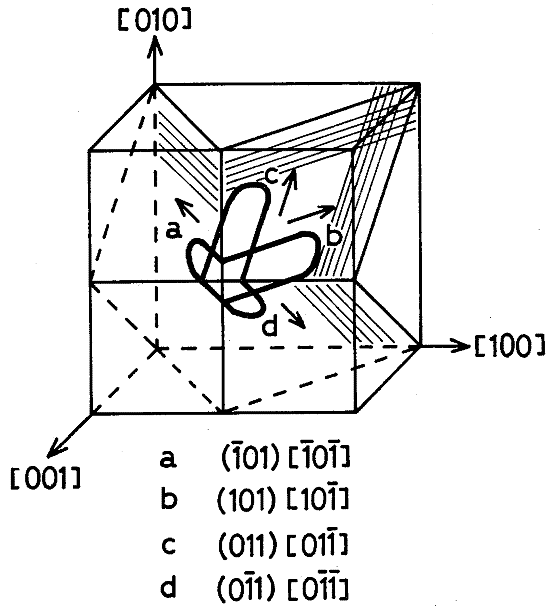

Fig. 1 Burgers vectors and crystallographic planes of laser-induced dislocations.

tively. Then half-loops revealed in (202) topograph must lie on $(\bar{1}01)$ plane. The crystallographic planes thus determined are listed in the last column in Table. 2. In Fig. 1 are shown the geometry of induced dislocations thus determined. A combination of Burgers vector and crystallographic plane shows that each half-loop is glissile dislocation.

Image contrast of dislocations thus determined will be examined in the case of diffraction vector $\boldsymbol{g}=[\bar{2}02]$ as shown in Fig. 2. Let $\angle \boldsymbol{g}\cdot\boldsymbol{b}$ be the angle be-

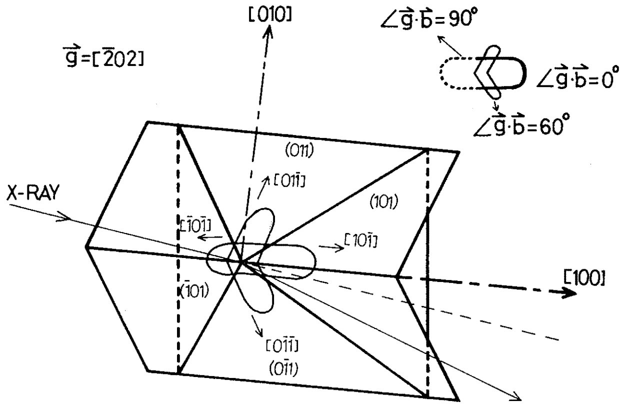

Fig. 2 Geometry for $(\bar{2}02)$ topograph. The loop $(\bar{1}01)$ $[\bar{1}0\bar{1}]$ is out of contrast because of invisibility criterion. Loops (101) $[10\bar{1}]$ and wing (011) $[01\bar{1}]$, $(0\bar{1}1)$ $[0\bar{1}\bar{1}]$ are observable as shown in Photo 2 (e).

tween vectors $\boldsymbol{g}$ and $\boldsymbol{b}$. For the half-loop of (101) $[10\bar{1}]$ $\angle \boldsymbol{g}\cdot\boldsymbol{b}=0°$ and excellent contrast is expected. While $\angle \boldsymbol{g}\cdot\boldsymbol{b}=90°$ for the half-loop $(\bar{1}01)$ $[\bar{1}0\bar{1}]$ and it is expected to be invisible. The half-loops of (011) $[01\bar{1}]$ and $(0\bar{1}1)$ $[0\bar{1}\bar{1}]$ are observable though they are inferior in contrast as $\angle \boldsymbol{g}\cdot\boldsymbol{b}=60°$ for these loops. The above examination well account for the result shown in Table 2 and Photo 2 (d) to (f).

Laser induced dislocations are concluded to be composed of four types of glissile dislocations in half-loops, (101) $[10\bar{1}]$, $(\bar{1}01)$ $[\bar{1}0\bar{1}]$, (011) $[01\bar{1}]$ and $(0\bar{1}1)$ $[0\bar{1}\bar{1}]$.

Acknowledgments

The author would like to acknowledge the continuing interest and encouragement of Dr. Futagami. He is grateful to Dr. Muraoka and Mr. Hiraki for providing a chance to use the laser system for irradiation. He is also indebted to Mr. Araki for his experimental assistance.

References

1) Akashi, Y., Dislocations Induced by Laser Irradiation, to be published in Japan. J. appl. Phys. Vol. 14, No. 11, 1975.
2) Hiraki, N., Kawasaki, S. and Muraoka, K., Infrared Laser Scattering System for the Plasma Diagnostics, Rep. Res. Inst. Appl. Mech., Vol. 23, No. 73, 1975, pp. 85-96.
3) Lang, A. R., Applications of 'Limited Projection Topographs' and 'Direct Beam Topographs' in Diffraction Topography, Brit. J. appl. Phys., Vol. 14, 1963, pp. 904-907.
4) Futagami, K., X-Ray Studies on the Sub-Grain Boundaries of LiF Single Crystals by the Limited Projection Topography, Japan. J. appl. Phys., Vol. 6, 1967, pp. 1381-1392.
5) Anderholm, N. C., Laser-Generated Stress Waves, appl. Phys. Letters, Vol. 16, 1970, pp. 113-115.

(Received September 30, 1975)

Appendix

According to the geometry of induced dislocations, a geometrical model was constructed. The model is photographed following the geometry of projection to take x-ray topography. The photographs corresponding to Photo 2 are shown in Photo Al. The invisibility criterion is not considered in these photograph. The following half-loops are invisible because of invisibility criterion, (011) and $(0\bar{1}1)$ in (a), $(\bar{1}01)$ and (101) in (b), (011) in (d), $(\bar{1}01)$ in (e) and (101) in (f). Comparing Photos 2 and Al, one can notice that the model well account for the topographs obtained.

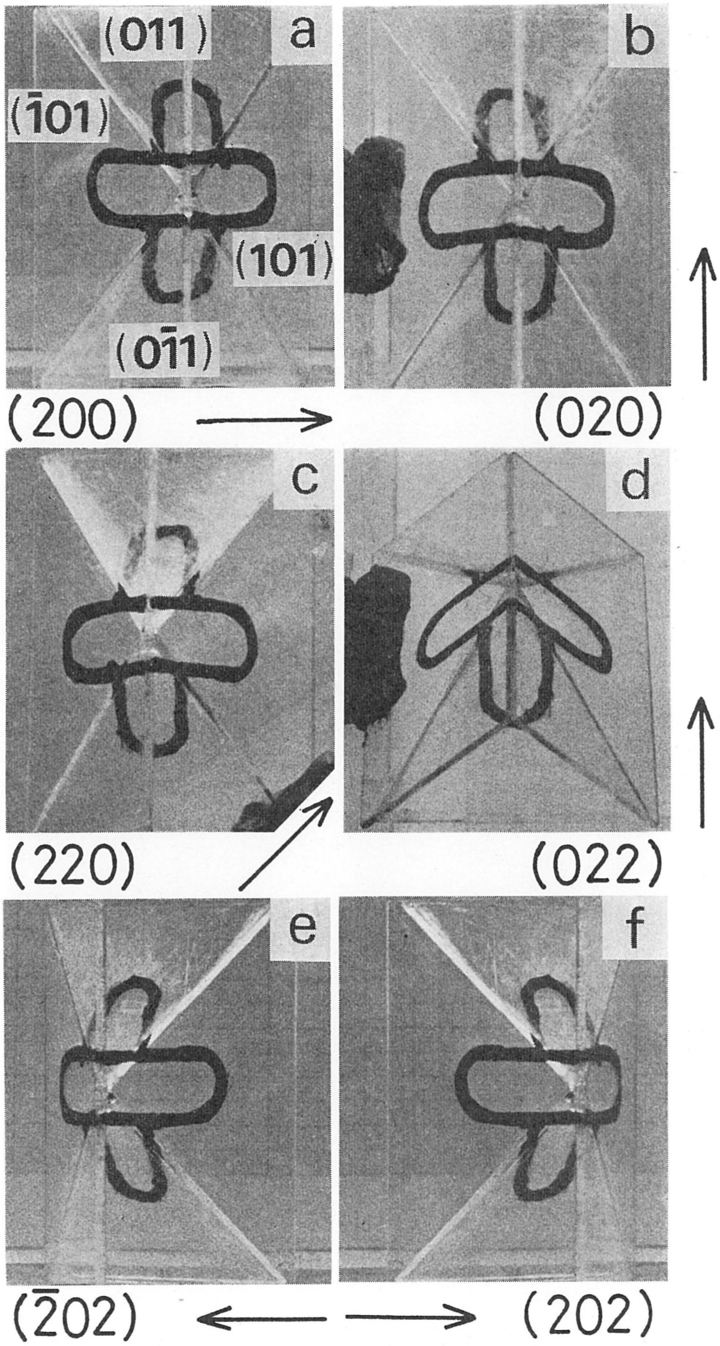

Photo A1 Photographs of the dislocation model obtained. Comparing these photographs with Photo 2, one can notice that the model well accouut for the topographs.